Aggregate fractal dimensions and thermal conduction in nanofluids

Patricia E. Gharagozloo[a] and Kenneth E. Goodson
Department of Mechanical Engineering, Stanford University, Stanford, California 94305, USA

(Received 9 March 2010; accepted 25 July 2010; published online 13 October 2010)

The mechanism producing enhanced thermal conductivities of nanofluids has been the subject of much debate. The formation of aggregates allowing for percolation paths within the fluid has shown the most promise. This work studies the aggregate formation of a nanofluid and compares the results to earlier thermal conductivity measurements and Monte Carlo simulation results. Static light scattering is employed to measure the fractal dimension of aggregates formed in the nanofluid over time at various temperatures and concentrations. As expected, aggregates form more quickly at higher concentrations and temperatures, which explains the increased enhancement with temperature reported by other research groups. The permanent aggregates in the nanofluid are found to have a fractal dimension of 2.4 and the aggregate formations that grow over time are found to have a fractal dimension of 1.8, which is consistent with diffusion limited aggregation. Predictions indicate that as aggregates grow the viscosity increases at a faster rate than thermal conductivity making the highly aggregated nanofluids unfavorable, especially at the low fractal dimension of 1.8. © *2010 American Institute of Physics*. [doi:10.1063/1.3481423]

I. INTRODUCTION

Nanofluids of metal and metal oxide nanoparticles suspended in fluids have generated much interest for electronics cooling applications due to reports of thermal conductivity enhancements much greater than those predicted. Effective medium theory (EMT) predicts for dilute suspensions of well-dispersed nanoparticles with $k_p \gg k_f$ a 3% increase for every $1\%_{\text{vol}}$ concentration. The high thermal conductivities reported could allow for large improvements in current fluidic system cooling abilities. The effect of temperature on the thermal conductivity of nanofluids has been highly controversial. Multiple research groups reported increased enhancements in the thermal conductivity with temperature but at varying intensity.[1–3] Other studies showed there is actually no direct increase in thermal conductivity with temperature and found the enhancements followed EMT well.[4–6] It is more likely another mechanism was causing the enhancements measured in the earlier studies possibly indirectly related to temperature. However, the actual mechanism has not yet been studied.

Effects of aggregation are found in the nanofluid studies by various research groups but are unaccounted for. Past measurements of viscosity showed increases of 10% or higher per $1\%_{\text{vol}}$ concentration.[7–11] This exceeds the predictions of Einstein in 1911 (Refs. 12 and 13) for well-dispersed nanoparticle suspensions of 2.5% per $1\%_{\text{vol}}$ concentration. Optical thermal conductivity measurements using forced Rayleigh scattering[14] and beam deflection[6] techniques yielded data consistent with EMT. Researchers that noted aggregation or opaque fluids with aggregates large enough to scatter light measured higher thermal conductivities than predicted by EMT.[1,15–17] Aggregation is the only mechanism of thermal conductivity enhancement that also accounts for the increases in viscosity. A recent benchmark study consisting of 34 research groups has shown that for a variety of stable, well-dispersed nanofluids, the thermal conductivity is well modeled through the Maxwell EMT.[18] Thus, aggregation is an important factor for thermal applications of any nanofluid. Prasher *et al.*[19] calculated the limit of nanofluid favorability to be when the ratio of the percent increase in viscosity to the percent increase in thermal conductivity is less than 4.

The enhancements achieved by aggregation depend on the aggregate size and structure. The progression of aggregation depends on the particle volume concentration and fluid temperature. An experimental and theoretical study of the aggregation progression and structure at various isothermal conditions is necessary for a full understanding of the thermal conductivity data and nanofluid favorability.

The effect of aggregation on thermal conductivity has been modeled by a few research groups. Calculations for typical aggregates give potential enhancements of 5% per $1\%_{\text{vol}}$ concentration for dense aggregates and up to 30% for sparse aggregates.[20–24] Prasher *et al.*,[25] showed the aggregation time constant to be inversely proportional to the fluid temperature and particle volume concentration and directly proportional to the fluid viscosity. If the concentration is doubled the particles will reach the same point in aggregation in half the time. As the temperature is increased the viscosity of the fluid decreases producing an even larger dependence on temperature. Philip *et al.*[17] measured the linear aggregation of stabilized magnetite particles in a magnetic field and measured an enhancement of 64%. Gao *et al.*[26] measured the thermal conductivity of clustering nanoparticles suspended in fluid and frozen. They found a 4% enhancement in the fluidic state and a 5% enhancement in the frozen state for $1\%_{\text{vol}}$ concentration, which they attributed to more structured aggregates when frozen. Chen *et al.*[27] measured enhancements in viscosity of 10% for $1\%_{\text{vol}}$ concentration and attributed the increase to aggregation. An experi-

[a]Present address: Sandia National Laboratories, P.O. Box 969, Livermore, CA 94551. Electronic mail: peghara@sandia.gov.

mental study of the aggregate structure and fractal dimension in heat transfer nanofluids has yet to be conducted.

In this paper, two experimental techniques are used to determine the initial state of the nanofluid and one experimental technique is used to study the aggregate progression and structure at various concentrations and temperatures. Dynamic light scattering (DLS) yields the initial particle size distribution and shows the presences of permanent aggregates in the nanofluid. Scanning electron microscopy (SEM) gives a visualization of the particles and permanent aggregates as they appear in suspension and allow for the calculation of their fractal dimension. Static light scattering gives the average fractal dimension of the aggregate formations over time at different length-scales for each of the volume concentrations at different temperatures. These results are compared to Monte Carlo simulations of aggregation, thermal conductivity and viscosity predictions, and previous experimental data of thermal conductivity over time. The methodology for the Monte Carlo simulation and thermal conductivity measurement are given by Gharagozloo and Goodson.[28] Finally, the favorability of aggregating nanofluids is analyzed.

II. MEASUREMENT THEORY

Static light scattering allows for the measurement of aggregate characteristics such as radius of gyration, fractal dimension, and primary particle size.[29–32] The magnitude of the scattering vector, q, of light scattered from a small particle is the difference between the incident wave vector, $\vec{k}_i$, and scattered wave vector, $\vec{k}_s$. Rayleigh scattering gives $|\vec{k}_i| = |\vec{k}_s| = 2\pi/\lambda$. For light scattered at angle, θ, the scattering vector is then given by[33]

$$q = \frac{4\pi n}{\lambda}\sin\left(\frac{\theta}{2}\right), \tag{1}$$

where n is the index of refraction of the base fluid and λ is the incident laser beam wavelength. The value $1/q$ represents the length scale sampled by the scattered light.

The intensity of the scattered light from an aggregate is given by $I(q) \propto P(q)S(q)$, where $P(q)$ is the form factor, which represents the intensity of scattered light from a single particle and $S(q)$ is the interparticle structure factor, which represents the added intensity from the light scattered between the particles in the aggregate and describes the structure of the aggregate. When $1/q < R_a$ the scattered light is considered in phase and when $1/q > R_a$ it is not. Variations in $I(q)$ are due mainly to $P(q)$ at large q and $S(q)$ at small q. For $R_a > 1/q > r_p$, $S(q)$ dominates the variation in $I(q)$ with respect to q. $S(q)$ varies as $n_q(N_q)^2$, where $N_q = c_i(qr_p)^{-d_f}$ is the number of scatterers in a particular q-region and $n_q = c_s(R_q q)^{d_f}$ is the number of q-regions, where c_i and c_s are constants and R_q is the length scale of q. This yields variations in intensity given by[34]

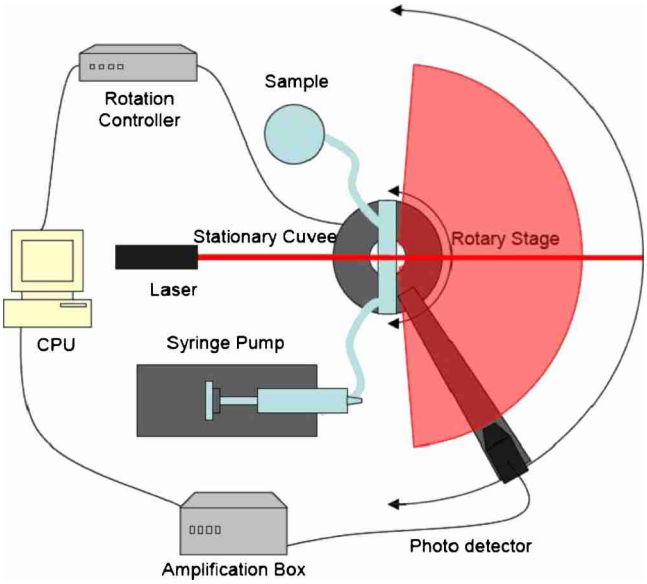

FIG. 1. (Color online) Schematic of static light scattering experimental setup showing nanofluid held in bottle at the specified temperature and at the measurement time is pulled into a stationary cuvee with a syringe pump. A laser is shone through the sample causing light to scatter. The scattered light intensity is measured vs angle using a photodetector attached to a rotary stage.

$$I(q) \propto \begin{cases} q^{-4} & 1/q < r_p \\ q^{-d_f} & R_a > 1/q > r_p \\ (R_a/r_p)^{d_f} & R_a < 1/q \end{cases}, \tag{2}$$

where R_a is the aggregate radius of gyration and r_p is the particle radius.

III. MEASUREMENT SETUP

A schematic of the experimental setup is shown in Fig. 1. The fluid is held in a stationary quartz spectrophotometer flow through cell (Starna/48-Q-0.5). A collimated 1 mW laser of wavelength 633 nm (Edmund Optics/NT59-080) or 785 nm (Edmund Optics/NT59-082) passes through the cell allowing the light to scatter off the aggregates. The scattered light intensity is measured by a 2.5 mm Si photodetector (Edmund Optics/NT57-624) detecting wavelengths from 200 to 1000 nm. The photodetector is rotated around the fluid cell with a motorized rotation stage (Newport/PR50PP) to measure the intensity versus angle. For each measurement, the fluid is heated to the desired temperature and pumped into the flow cell by syringe. The refraction from the water/quartz/air interfaces are accounted for in the angle used to determine the scattering vector. With the 785 nm laser source we sample the length scale from 150 to 180 nm and with the 633 nm laser source we sample the length scale from 115 to 140 nm.

The measurement is verified in three ways. First, the variation is confirmed to be symmetric as the measurement is done in both the positive and negative direction. Second, the correct measurement of larger solid amorphous silica National Institute of Standards and Technology (NIST) traceable size standards particles (Thermo Scientific/8050) in the $1/q < r_p$ regime is confirmed. Third, the measurements of the

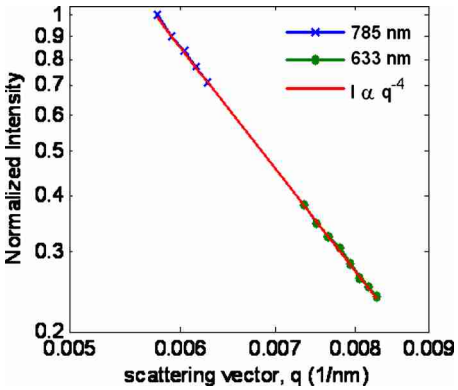

FIG. 2. (Color online) Log-log plot of the normalized intensity versus scattering vector for the NIST traceable size standards showing the -4 power law for $1/q < r_p$ (red line). Amorphous silica particles, 0.5 μm in diameter dispersed in water are measured with the 785 nm laser (blue x's) and with the 633 nm laser (green dots).

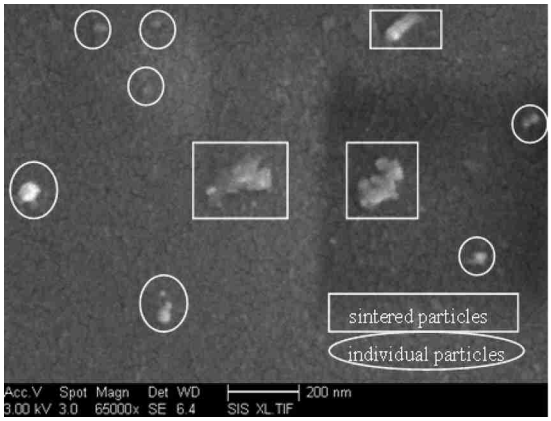

FIG. 4. SEM image of suspended alumina nanoparticles from the gelified water based nanofluid showing the presence of singlet particles and permanent aggregates of particles sintered together.

NIST traceable size standards and permanent aggregates are made with two lasers (633 and 785 nm) of different wavelength to ensure the same values are measured. The intensity versus scattering vector data for the NIST traceable size standard particles are plotted in Fig. 2.

The nanofluid has 20% weight concentration alumina in H_2O with less than 1% nitric acid (Alfa Aesar/12733). The fluid is diluted with deionized water to the desired volume concentrations. The *p*H of each of the concentrations is measured to be 5.5 to ensure the chemistry is constant between each of the samples. Prior to the measurements the nanofluid is sonicated for 4 h. To prevent variations in the lapse in time between sonication and the measurement the fluid is heated to the desired temperature during sonication. An estimated 15 min elapses between sonication and measurement for each case as the fluid is loaded into the light scattering setup and flow effects are allowed to subside. The nanofluid is stable with only minor settling after a week. DLS measurements are performed using the 90Plus Particle Analyzer from Brookhaven Instruments Corporation on a solution diluted to $0.05\%_{\text{vol}}$ concentration and the results are shown in Fig. 3 for both the intensity and number based multimodal distributions. The DLS yields a nominal particle diameter of 40 nm and skew of 11.5 nm. A small number of sintered particles are initially present with a nominal diameter of 125 nm as shown with the intensity based DLS distribution. A subset of the sintered particles is large enough to scatter visible light though the fluid remains mostly transparent. The sintered particles will be at a higher fractal dimension than the diffusion limited aggregates and the measured fractal dimension will be an average of the fractal dimensions from the aggregates at the length scale sampled.

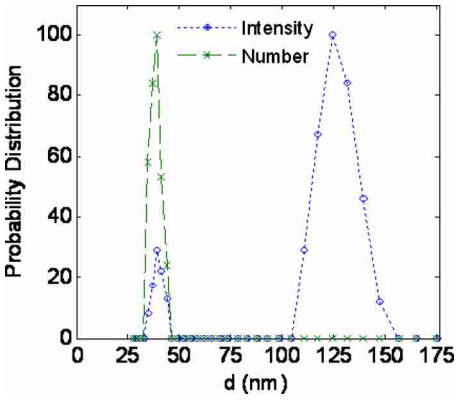

FIG. 3. (Color online) Multimodal particle size distributions from DLS for nanofluid of alumina in water diluted to 0.05% volume concentration presented in both number and intensity based distributions to show presence of permanent aggregates.

A FEI XL30 Sirion SEM with field emission gun source is used to image the particles as they are in suspension to observe individual particle aggregates. To view nanofluids in a SEM and keep the particles suspended, the nanofluids are subjected to a jellification and hardening process. Enüstün and Turkevich[35] found gelatin to be an effective coagulation stopping agent to allow viewing of particles at various stages of coagulation. Fernández-Morán and Finean[36] used gelatin for embedding small, fragile samples, for viewing in an electron microscope. To create the gelified nanofluid, the nanofluid is sonicated, heated to 40 °C and mixed at a 1:2 volume ratio with a 40 °C 15% by weight gelatin—deionized H_2O solution. A thin layer of the mixture is poured into a clean dish and placed in a refrigerator for 30 min to allow the mixture to gelify and is then transferred into a vacuum chamber for 6 h to remove any excess liquid from the nanogel film. An image of the nanoparticles is shown in Fig. 4.

The fractal dimension of the sintered aggregates is estimated from the SEM image. The image is converted to binary changing the pixels within the particles to white and the pixels outside the particle to black as shown in Fig. 5. A circle is drawn around the particle to just include the aggregate and all the pixels outside the circle are not counted. The concentration of particles in the aggregate is estimated as the ratio of the number of white pixels to total pixels in the circle and is found to be 0.51. We estimate the fractal dimension of the initial sintered aggregates to be 2.5 ± 0.1 from the following equation:

FIG. 5. Binary version of aggregate from SEM image. The particle volume fraction in the aggregate is estimated from this image to be 0.51.

$$\varphi_{p,agg} = \left(\frac{2R_a}{d_p}\right)^{d_f-3}, \tag{3}$$

where $\varphi_{p,agg}$ is the particle volume fraction in the aggregate, R_a is the aggregate radius, d_p is the particle diameter, and d_f is the fractal dimension.

The Monte Carlo simulation models the aggregation over time in isothermal conditions. To further understand the effect of aggregation on the fluid properties the thermal conductivity and viscosity are modeled using fractal theory. The thermal conductivities of the aggregates are calculated by separating them into two components, the percolation contributing backbone, and nonpercolation contributing dead-ends.[25] The effective thermal conductivity of the dead-end particles, k_{nc}, is calculated using the Bruggeman model, which is appropriate for high particle volume fractions[37]

$$\sum_i \frac{\varphi_i(k_i - k_{nc})}{k_i + 2k_{nc}} = 0, \tag{4}$$

where φ_i is the volume fraction of the nonpercolation contributing aggregate components (fluid and dead-end particles) and k_i is the thermal conductivity of the components. The effective thermal conductivity of the aggregate, k_{agg}, is calculated using composite theory for misoriented ellipsoidal particles for the backbone, in a matrix of the nonpercolation contributing portion. The following equations are used:[38]

$$k_{agg} = k_{nc}\frac{3 + \varphi_c[2\beta_{11}^c(1-L_{11}) + \beta_{33}^c(1-L_{33})]}{3 - \varphi_c(2\beta_{11}^c L_{11} + \beta_{33}^c L_{33})}, \tag{5}$$

$$L_{11} = \begin{cases} 0.5p^2/(p^2-1) - 0.5p\cosh^{-1}p/(p^2-1)^{1.5} & p > 0 \\ 1/3 & p = 0 \end{cases}, \tag{6}$$

$$L_{33} = 1 - 2L_{11}, \tag{7}$$

$$\beta_{ii}^c = (k_{ii}^c - k_{nc})/[k_{nc} + L_{ii}(k_{ii}^c - k_{nc})] \quad i = 1,3, \tag{8}$$

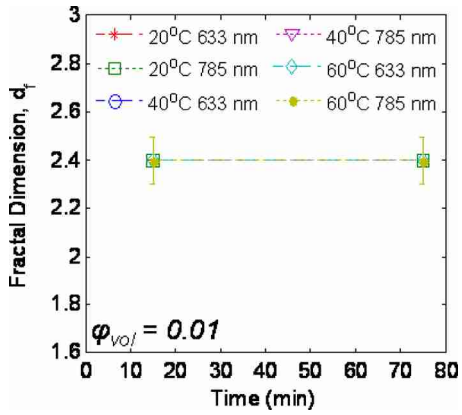

FIG. 6. (Color online) Plot of the fractal dimension versus time for the 1% volume concentration of 40 nm alumina nanoparticles in water at 20, 40, and 60 °C.

$$k_{ii}^c = \frac{k_p}{(1 + \gamma L_{ii}k_p/k_f)}, \quad \left[\text{with } \gamma = \left(2 + \frac{1}{p}\right)\alpha, \quad \alpha = \frac{2R_b k_f}{d_p}\right], \tag{9}$$

where R_b is the boundary resistance between the particle and the fluid and p is the ratio between the radius of the aggregate to the radius of the particle. In a previous study the typical boundary resistance between alumina and water was found to reduce the thermal conductivity by less than 5%.[28] In this study the boundary resistance is assumed to be zero. The effective thermal conductivity of the nanofluid is found through the Maxwell EMT[39] for dispersed particles and is given by

$$k_{eff} = k_f\frac{k_{agg} + (n-1)k_f - (n-1)\varphi_{agg}(k_f - k_{agg})}{k_{agg} + (n-1)k_f + \varphi_{agg}(k_f - k_{agg})}, \tag{10}$$

where φ_{agg} is the volume fraction of aggregates in the fluid and $n = 3/\psi$, where ψ is the sphericity of the aggregate. A spherical aggregate is assumed yielding $n=3$. The bulk effective hydrodynamic viscosity for a fluid containing fractal aggregates is modeled by Potanin[40] and is given by

$$\mu_{eff} = \mu_f\left(1 - \frac{\varphi_{agg}}{\varphi_{\max}}\right)^{-2.5\varphi_{\max}}, \tag{11}$$

where $\varphi_{\max} = 0.61$ is the maximum possible volume concentration for rigid spheres. This equation is most appropriate for higher shear rates, but is a good approximation since most nanofluids have been found to have limited shear thinning. Both of these equations are dependent on the fractal dimension of the aggregates.

IV. RESULTS AND DISCUSSION

The measured fractal dimensions for the 1%, 3%, and 5% volume concentrations are shown in Figs. 6–8, respectively, at 20 °C, 40 °C, and 60 °C after sonication and an hour after being held at the specified temperatures. The 1% volume concentration shows a fractal dimension of 2.4 at all times and temperatures due to a lack of significant aggregation. The 3% volume concentration shows a fractal dimen-

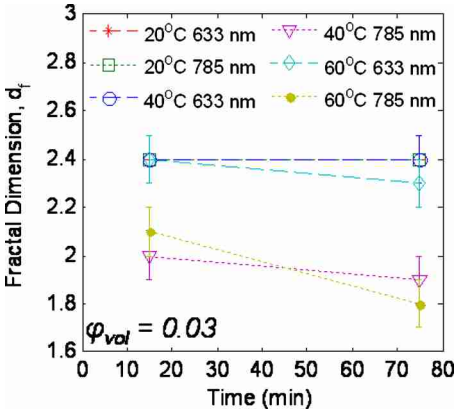

FIG. 7. (Color online) Plot of the fractal dimension versus time for the 3% volume concentration of 40 nm alumina nanoparticles in water at 20, 40, and 60 °C.

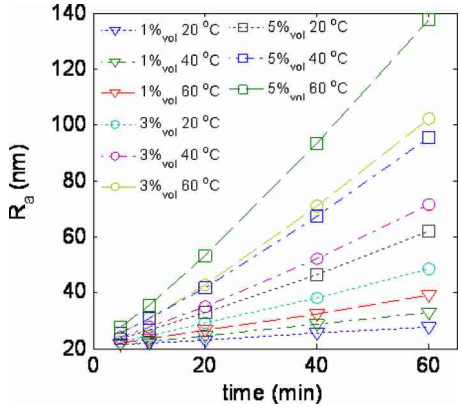

FIG. 9. (Color online) Simulated average radius of gyration of the aggregates over time for 1%, 3%, and 5% volume concentrations at 20, 40, and 60 °C.

sion of 2.4 for 20 °C at both times and wavelengths. At 40 °C at the smaller length-scales below 135 nm, the fractal dimension is 2.4 and at larger length-scales the average fractal dimension becomes 2.0 at early times and reduces to 1.9 after an hour. At 60 °C at the smaller length-scales, the average fractal dimension begins at 2.4 and reduces to 2.3 after an hour. At the larger length-scales, the average fractal dimension begins at 2.1 and reduces to 1.8 after an hour. The 5% volume concentration again shows a fractal dimension of 2.4 for 20 °C at both times and length-scales and for 40 °C at the smaller length-scales initially and then reduces to 2.3 after an hour. At 60 °C at the smaller length-scales the average fractal dimension begins at 2.2 and reduces to 2.0 after an hour. At the larger length-scales the average fractal the average fractal dimension becomes 1.8 at both 40 and 60 °C at both times.

Plotted in Fig. 9 is the modeled average radius of gyration from a Monte Carlo simulation modeling the aggregation in isothermal conditions with an assumed fractal dimension of 1.8 for each of the concentrations and temperatures. For the 1% volume concentration the average radius of the aggregates stays smaller than the size of the permanent aggregates in the fluid. These results are consistent with the measurement since not enough aggregation has occurred to influence the measured average fractal dimension. For the 3% volume concentration, the aggregates remain small for the 20 °C case. At 40 °C, the aggregates begin to become as large as and larger than the permanent aggregates. This is consistent with the measurements where the average fractal dimension begins to be influenced by the aggregate formations. At the larger length scale, very few permanent aggregates are present and the average fractal dimension is much more affected by the aggregate formations and decreases more rapidly. At 60 °C, the aggregation occurs more quickly and the measured average fractal dimension is affected even at the smaller length-scales. For the 5% volume concentration, the aggregate formations are predicted to increase to the size of the permanent aggregates at 20 °C, however the measurement show no effect. At 40 °C the aggregate formations become larger than the permanent aggregates and are about the same as the 60 °C case for the 3% volume concentration. This is consistent with the average fractal dimension measurements which are about the same for the two cases. At 60 °C, the average aggregate size is over twice as large as the permanent aggregates and much more aggregation has occurred, which is consistent with the average fractal dimension measurements with the average fractal dimension reducing for both length-scales.

The ratio of the increase in viscosity to the increase in

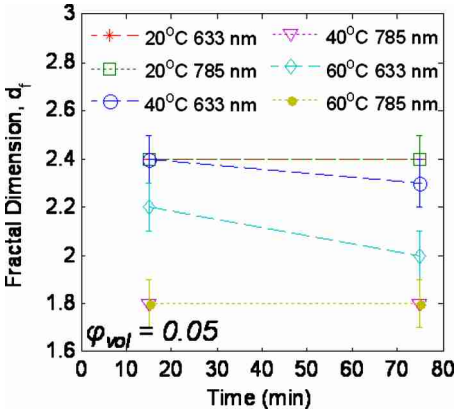

FIG. 8. (Color online) Plot of the fractal dimension versus time for the 5% volume concentration of 40 nm alumina nanoparticles in water at 20, 40, and 60 °C.

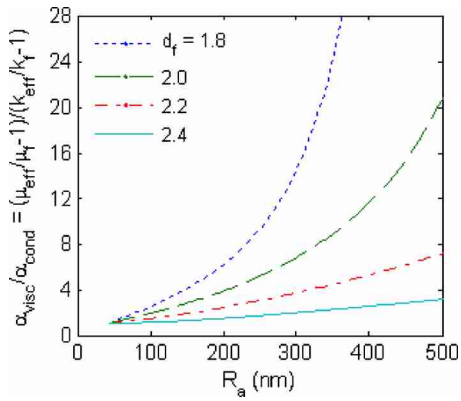

FIG. 10. (Color online) Ratio of viscosity to thermal conductivity enhancement vs aggregate radius of gyration for 40 nm alumina nanoparticles in water for various fractal dimensions.

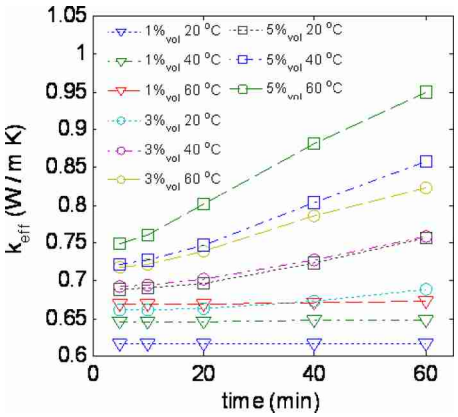

FIG. 11. (Color online) Thermal conductivity plotted over time for the three concentrations each at the three temperatures calculated from the volume average of the simulated aggregate radius of gyration for a fractal dimension of 1.8 in a nanofluid with 40 nm alumina nanoparticles dispersed in water.

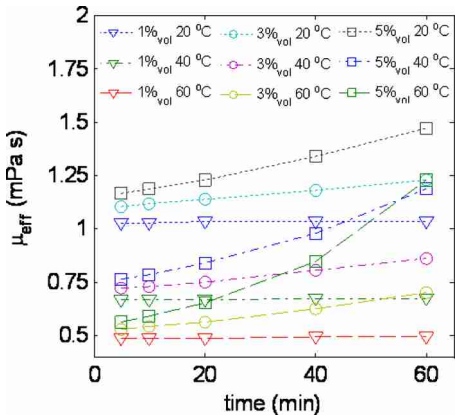

FIG. 13. (Color online) Viscosity plotted over time for the three concentrations each at the three temperatures calculated from the volume average of the simulated aggregate radius of gyration for a fractal dimension of 1.8 in a nanofluid with 40 nm alumina nanoparticles dispersed in water.

thermal conductivity for different fractal dimensions is plotted versus aggregate size in Fig. 10. This assumes all aggregates are the same size and no singlet particles are present. At higher fractal dimensions the aggregates are denser causing less volume to be consumed by the aggregates yielding smaller effects on the fluid properties.

The thermal conductivity and viscosity are calculated using the predicted distribution of aggregate sizes from the Monte Carlo simulation is used through a volumetric average. The calculated thermal conductivity over time for each case is plotted in Fig. 11. The thermal conductivity from previous experiments[41] is plotted in Fig. 12. The average temperature in the experiments was 50 °C with about a 25 °C temperature variation across the sample. The results from the measurement agree well with the Monte Carlo results for aggregation. The calculated viscosity over time for each case is plotted in Fig. 13. The plot shows that aggregation can cause the increase in viscosity to reach and surpass 10% per 1% volume fraction. The ratio of the viscosity increase to the thermal conductivity increase over time is plotted in Fig. 14 for each case. As aggregation progresses both the thermal conductivity and viscosity rise. Initially the thermal conductivity rises as fast as the viscosity; however, once the aggregates become large the viscosity increases much faster than the thermal conductivity creating an unfavorable nanofluid for heat transfer. From the work of Potanin *et al.*,[40] it is expected that in shear conditions the aggregates will compress. They showed increases in the fractal dimension from 1.8 to 2.3 in oscillating shear flows. Even with diffusion limited aggregation the nanofluid could remain favorable up to large aggregate sizes but would likely eventually become unfavorable as aggregation continued to progress.

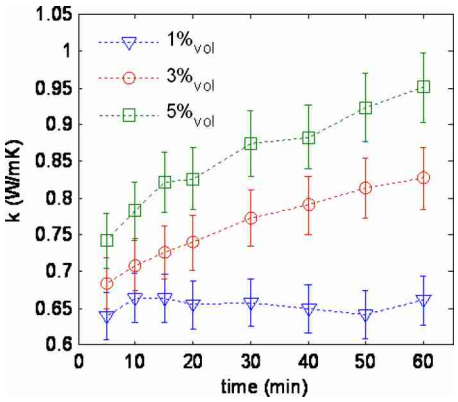

FIG. 12. (Color online) Plot of the measured time dependence of the average thermal conductivity for the three concentrations of nanofluid consisting of 40 nm alumina nanoparticles in water (Ref. 41).

V. CONCLUDING REMARKS

At room temperature this fluid is well stabilized and very little aggregate formations are present over time. When the nanofluid is heated the nanoparticles experience stronger Brownian motion. This allows for greater aggregation at higher temperatures. At higher concentrations, more particles are present allowing particles to interact more, increasing the amount of aggregation. The diffusion limited aggregation produces fractal dimensions of 1.8, which is especially apparent in the higher concentrations and temperatures in the length scale larger than the permanent aggregates.

These results show that aggregation is a more likely cause for the measured enhancements with temperature by

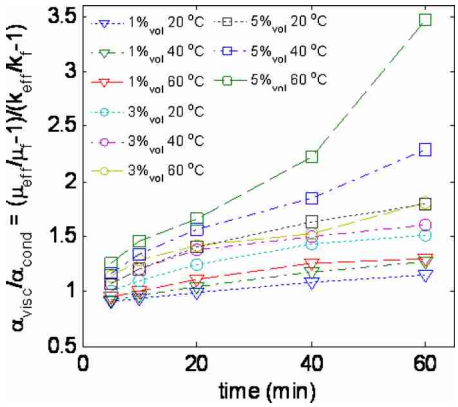

FIG. 14. (Color online) Ratio of the viscosity to thermal conductivity enhancements plotted over time for the three concentrations each at the three temperatures calculated from the volume average of the simulated aggregate radius of gyration for a fractal dimension of 1.8 in a nanofluid with 40 nm alumina nanoparticles dispersed in water.

previous research groups. At higher temperatures, aggregation occurs quick enough to effect measurements within minutes of sonication. If the fluid is not heated during sonication and must be heated between sonication and the measurement the aggregation would progress further for the higher temperatures with more time lapse.

ACKNOWLEDGMENTS

The authors acknowledge the financial support from the Office of Naval Research through Contract No. N00014-05-0374-P00001 and graduate fellowships from the National Science Foundation and Sandia National Laboratories.

[1]S. K. Das, N. Putra, P. Thiesen, and W. Roetzel, J. Heat Transfer **125**, 567 (2003).
[2]H. E. Patel, S. K. Das, T. Sundararajan, A. S. Nair, B. George, and T. Pradeep, Appl. Phys. Lett. **83**, 2931 (2003).
[3]C. H. Li and G. P. Peterson, J. Appl. Phys. **99**, 084314 (2006).
[4]X. Zhang, H. Gu, and M. Fujii, Int. J. Thermophys. **27**, 569 (2006).
[5]B. Yang and Z. H. Han, Appl. Phys. Lett. **89**, 083111 (2006).
[6]D. C. Venerus, M. S. Kabadi, S. Lee, and V. Perez-Luna, J. Appl. Phys. **100**, 094310 (2006).
[7]J.-F. Zhao, Z.-Y. Luo, M.-J. Ni, and K.-F. Cen, Chin. Phys. Lett. **26**, 066202 (2009).
[8]W. J. Tseng and C. H. Wu, Acta Mater. **50**, 3757 (2002).
[9]J.-H. Lee, K. S. Hwang, S. P. Jang, B. H. Lee, J. H. Kim, S. U. S. Choi, and C. J. Choi, Int. J. Heat Mass Transfer **51**, 2651 (2008).
[10]J. Garg, B. Poudel, M. Chiesa, J. B. Gordon, J. J. Ma, J. B. Wang, Z. F. Ren, Y. T. Kang, H. Ohtani, J. Nanda, G. H. McKinley, and G. Chen, J. Appl. Phys. **103**, 074301 (2008).
[11]J. Lee, P. E. Gharagozloo, B. Kolade, J. K. Eaton, and K. E. Goodson, J. Heat Transfer **132**, 092401 (2010).
[12]A. J. Hughes, Nature **173**, 1090 1954).
[13]A. Einstein, Ann. Phys. **339**, 591 (1911).
[14]A. Putnam, D. G. Cahill, P. V. Braun, Z. Ge, and R. G. Shimmin, J. Appl. Phys. **99**, 084308 (2006).
[15]J. A. Eastman, S. U. S. Choi, S. Li, L. J. Thompson, and S. Lee, MRS Symposia Proceedings No. 457 (Materials Research Society, Pittsburgh 1997), p. 3.
[16]M.-S. Liu, M. C.-C. Lin, C. Y. Tsai, and C.-C. Wang, Int. J. Heat Mass Transfer **49**, 3028 (2006).
[17]J. Philip, P. D. Shima, and B. Raj, Nanotechnology **19**, 305706 (2008).
[18]J. Buongiorno, D. C. Venerus, N. Prabhat, T. McKrell, J. Townsend, R. Christianson, Y. V. Tolmachev, P. Keblinski, L.-W. Hu, J. L. Alvarado, I. C. Bang, S. W. Bishnoi, M. Bonetti, F. Botz, A. Cecere, Y. Chang, G. Chen, H. Chen, S. J. Chung, M. K. Chyu, S. K. Das, R. D. Paola, Y. Ding, F. Dubois, G. Dzido, J. Eapen, W. Escher, D. Funfschilling, Q. Galand, J. Gao, P. E. Gharagozloo, K. E. Goodson, J. G. Gutierrez, H. Hong, M. Horton, K. S. Hwang, C. S. Iorio, S. P. Jang, A. B. Jarzebski, Y. Jiang, L. Jin, S. Kabelac, A. Kamath, M. A. Kedzierski, L. G. Kieng, C. Kim, J.-H. Kim, S. Kim, S. H. Lee, K. C. Leong, I. Manna, B. Michel1, R. Ni, H. E. Patel1, J. Philip, D. Poulikakos, C. Reynaud, R. Savino, P. K. Singh, P. Song, T. Sundararajan, E. Timofeeva, T. Tritcak, A. N. Turanov, S. V. Vaerenbergh, D. Wen, S. Witharana, C. Yang, W.-H. Yeh, X.-Z. Zhao, and S.-Q. Zhou, J. Appl. Phys. **106**, 094312 (2009).
[19]R. Prasher, D. Song, J. Wang, and P. Phelan, Appl. Phys. Lett. **89**, 133108 (2006).
[20]R. Prasher, W. Evans, P. Meakin, J. Fish, P. Phelan, and P. Keblinski, Appl. Phys. Lett. **89**, 143119 (2006).
[21]J. Eapen, J. Li, and S. Yip, Phys. Rev. E **76**, 062501 (2007).
[22]B. Wang, L. Zhou, and X. Peng, Int. J. Heat Mass Transfer **46**, 2665 (2003).
[23]J. A. Eastman, S. R. Phillpot, S. U. S. Choi, and P. Keblinski, Annu. Rev. Mater. Res. **34**, 219 (2004).
[24]W. Evans, R. Prasher, J. Fish, P. Meakin, P. Phelan, and P. Keblinski, Int. J. Heat Mass Transfer **51**, 1431 (2008).
[25]R. Prasher, P. Phelan, and P. Bhattacharya, Nano Lett. **6**, 1529 (2006).
[26]J. W. Gao, R. T. Zheng, H. Ohtani, D. S. Zhu, and G. Chen, Nano Lett. **9**, 4128 (2009).
[27]H. Chen, Y. Ding, and C. Tan, New J. Phys. **9**, 367 (2007).
[28]P. E. Gharagozloo and K. E. Goodson, "Temperature-dependent aggregation and diffusion in nanofluids," Int. J. Heat Mass Transfer (to be published).
[29]G. Bushell and R. Amal, J. Colloid Interface Sci. **221**, 186 (2000).
[30]D. W. Schaefer, J. E. Martin, P. Wiltzius, and D. S. Cannell, Phys. Rev. Lett. **52**, 2371 (1984).
[31]A. J. Salem and G. G. Fuller, J. Colloid Interface Sci. **108**, 149 (1985).
[32]D. A. Weitz, J. S. Huang, M. Y. Lin, and J. Sung, Phys. Rev. Lett. **54**, 1416 (1985).
[33]C. M. Sorensen, Aerosol Sci. Technol. **35**, 648 (2001).
[34]G. C. Bushell, Y. D. Yan, D. Woodfield, J. Raper, and R. Amal, Adv. Colloid Interface Sci. **95**, 1 (2002).
[35]B. V. Enüstün and J. Turkevich, J. Am. Chem. Soc. **85**, 3317 (1963).
[36]H. Fernández-morán and J. B. Finean, J. Biophys. Biochem. Cytol. **3**, 725 (1957).
[37]R. Landauer, AIP Conf. Proc. **40**, 2 (1978).
[38]C.-W. Nan, R. Birringer, D. R. Clarke, and H. Gleiter, J. Appl. Phys. **81**, 6692 (1997).
[39]J. C. Maxwell, *A Treatise on Electricity and Magnetism*, 2nd ed. (Clarendon, Oxford, 1881), p. 365.
[40]A. A. Potanin, R. De Rooij, D. Van den Ende, and J. Mellema, J. Chem. Phys. **102**, 5845 (1995).
[41]P. E. Gharagozloo, J. K. Eaton, and K. E. Goodson, Appl. Phys. Lett. **93**, 103110 (2008).